ELSEVIER

Contents lists available at ScienceDirect

Process Safety and Environmental Protection

journal homepage: www.journals.elsevier.com/process-safety-and-environmental-protection





The analysis and optimization of S-CO₂ coal fired power generation system using the split method

Yuandong Guo^a, Enhui Sun^{a,*}, Jinliang Xu^a, Cheng Chang^a, Zhaofu Wang^b

- a Key Laboratory of Power Station Energy Transfer Conversion and System, North China Electric Power University, Ministry of Education, Beijing 102206, China
- ^b China Three Gorges Corporation Institute of Science and Technology, Beijing 101199, China

ARTICLE INFO

Keywords: S-CO₂ cycle Coal-fired power plant Split method Complicated cycle analysis Converting low-grade heat into high-grade heat

ABSTRACT

The split method effectively elucidates the structural characteristics of complex power generation systems by analyzing the distribution of cycle flow rates. However, it is still primarily focused on the analysis of the supercritical carbon dioxide (S-CO₂) cycle. In this paper, the split method was first applied to the performance analysis of S-CO₂ coal-fired complicated power generation system. Taking tri-compressions S-CO₂ cycle with reheating process (TC+RH) as an example, the impact of the flue gas cooler method (FGC) on cycle was described more simply. TC+RH+FGC was equivalent to adding an inefficient sub-cycle to TC+RH, Therefore, applying FGC did not improve the thermal efficiency. This finding prompted us to optimize the new sub-cycle. Then, a method for converting low-grade heat into high-grade heat (CLH) was originally proposed. After the dry-cooler heat was recovered to boiler, this portion of heat is reused in the form of flue gas to heat the new sub-cycle, and the boiler efficiency remains constant. When the thermal efficiency of TC+RH was 51.38 %, that of the new sub-cycle was 61.30 %. Therefore, the thermal efficiency of the overall system reached 52.41 %. This study illustrates the advantages of the split method for analyzing complicated coal-fired power generation systems.

1. Introduction

As a signatory to the Paris Agreement, China has international obligations to contribute to the global effort to limit warming to well below 2 °C (Guo et al., 2022; Lu et al., 2023). The Coal-fired power generation accounts for over 40 % of Chinese electricity production, and the steam Rankine cycle is commonly employed in coal-fired power plants (Wang et al., 2023). Due to the cost limitations of metal materials, the efficiency improvement of the Rankine cycle faces challenges (Wang et al., 2022). In contrast, when the main vapor temperature is higher than 550 °C, the supercritical carbon dioxide (S-CO2) Brayton cycle is more efficient (Li et al., 2024; Sun et al., 2024). It has following benefits: (1) CO2 is more indolent than water. The mass increase due to surface oxidation is smaller for CO2 compared to water vapor when interacting with metal materials (Holcomb et al., 2016); (2) The S-CO2 cycle is compact, making it attractive for peak-shaving applications (Zhang et al., 2022); (3) CO₂ has a lower critical temperature (30.98 °C), so that more readily reaches its critical point (Wang et al., 2020b).

The single recuperator S-CO₂ cycle (SC) emerged in the 1960s, primarily out of the works of (Feher, 1968). However, it did not become a research hotspot. With the breakthrough of core components, (Dostál,

(Xu et al., 2018) pointed out that, when the S-CO $_2$ cycle is coupled with a coal-fired heat source, the flue gas heat in full temperature zone is difficult to be absorbed (Ramos da Costa et al., 2012). In order to solve this problem, the system needs to be optimized. For example, adopting top-bottom-combined cycle (Sun et al., 2018), using multiple heat sources to replace the partial heat loads of the flue gas (Sun et al., 2019), and using the most common method, flue gas cooler (FGC) method, to absorb flue gas heat (Hanak et al., 2020). The FGC method was proposed by (Mecheri and Le Moullec, 2016), which extracts a portion of CO $_2$ from the cycle into the FGC for absorbing low-temperature flue gas heat, and then returns to the cycle. Although the issue of flue gas residual heat

²⁰⁰⁴⁾ coupled nuclear energy with S-CO $_2$ cycle and conducted detailed system design and thermodynamic analysis. Since then, more scholars have been researching S-CO $_2$ cycle (Ahn et al., 2015; Gu et al., 2020; Turchi et al., 2013; Yang et al., 2022). Numerous studies have focused on S-CO $_2$ cycle powered by various energy sources, including nuclear energy (Wu et al., 2020), waste heat (Alfani et al., 2024; Ruiz-Casanova et al., 2020), natural gas (Liese et al., 2020), solar energy (Hadelu et al., 2022; Milani et al., 2017; Narasiah et al., 2024), coal-fired (Wang et al., 2020a; Zhou et al., 2018) and geothermal energy (Wu et al., 2018). Due to the focus of this study on the complicated S-CO $_2$ coal-fired plant, further research on other heat sources will not be introduced here.

^{*} Correspondence to: North China Electric Power University, Baoding, China. E-mail address: ehsun@ncepu.edu.cn (E. Sun).

Nomenclature		WC	wet-cooler
		x	split ratio
AP C CLH DC FGC HTR HFGC h LTR LFGC MFGC MTR m P Q q RC	air preheater compressor low-grad convert to high-grad heat dry-cooler flue gas cooler high temperature recuperators high temperature FGC enthalpy per unit mass, kJ/kg low temperature recuperator low temperature FGC medium temperature FGC medium temperature recuperator mass flow rate, kg/s pressure, MPa thermal load, MW heat absorption, kW/kg recompression cycle	x Subscripts 1, 2, 3 0 a b e ex f fg p pri R RR re s sec	split ratio s state points environment heat absorption boiler electric power exhaust lower heating value flue gas pipeline primary heat released RC+RH recovery isentropic secondary
RH S-CO ₂	reheating supercritical carbon dioxide	TR th	TC+RH thermal
sub T T TC W	simple regenerative turbine temperature, °C tri-compressions cycle output/input work, MW	Greek syr η α Δ	nbols efficiency boiler heat retention coefficient difference

has been resolved, the complexity of the cycle structure will inevitably increase. This means that it is difficult for us to simply explain the impact of FGC method on the cycle. For example, (Zhang et al., 2018) and (Park et al., 2018) have drawn opposing conclusions regarding two different S-CO₂ cycles coupled with FGC. (Mecheri and Le Moullec, 2016) adopted a new FGC arrangement and achieved optimal efficiency.

To sum up, the above studies show that there are some variations in perceptions of the FGC. Conventional analysis methods are difficult to clearly understand the effect of different FGC methods on cycle performance. We prefer to use simple analytical methods to understand complex cycle. Then, the split method was applied to understand the role of the FGC.

The split method, proposed by (Sun et al., 2020), is a method to split a complex cycle into multiple sub-cycles through the distribution of cycle working fluid flow rate. Then, the performance evaluation of the complex cycle can be equivalent to the thermodynamic performance evaluation of sub-cycles. Compared with the conventional cycle performance analysis method, the split method can be used to analyze the performance characteristics of complicated systems more simply and clearly (Zhao et al., 2021). For example, (Sun et al., 2020) applied the split method to split the RC into two simple regenerative sub-cycles. In this way, the reason why RC is more efficient than SC is revealed, that is, RC can be equivalent to adding a new sub-cycle with 100 % efficiency to SC. (Xin et al., 2020) also applied the split method to analyze the S-CO₂ cycle and process of intercooling and reheating. In recent research, the application of the split method is still limited to cycle analysis instead of the coupling between the cycle and the heat source. In this context, it is found that there is room for future study by reviewing the split method.

The innovations of this study are as follows: (1) Using new analytical method to more clearly reveal the essence of the FGC method; (2) The method for converting low-grade heat into high-grade heat (CLH) was proposed to improve the thermal efficiency of the new sub-cycle. Taking tri-compressions cycle with reheating (TC+RH) combined with three different FGC methods (LFGC, MFGC, HFGC) as an example, the system was decoupled by adding a new sub-cycle on the basis of TC+RH. Since the thermal efficiency of the new sub-cycle is not higher than that of

TC+RH, the thermal efficiency of TC+RH+FGC will not improve. To address this issue, the CHL method was proposed. The cooler waste heat was used to replace part of flue gas heat for heating air, and the replaced flue gas heat was then used to heat the sub-cycle. Therefore, the thermal efficiency of the new sub-cycle was improved.

This paper is divided into five chapters. Assumptions of the present paper and numerical model for the system are described in Section 2. In Section 3, the effect of different FGC methods on the cycle efficiency is analyzed by applying the split method. In Section 4, the CLH method is applied to improve the thermal efficiency of the new sub-cycle. The main conclusions are summarized in Section 5.

2. Analysis of complex coal-fired power generation systems

$2.1. \ \ Heat \ absorption \ problem \ of \ flue \ gas$

Fig. 1 shows a schematic diagram of energy transfer in the coal-fired power generation system. The grey lines represent the mass flow, the red lines represent the energy flow in heat absorption side and the blue lines represent the energy flow in heat released side. The combustion of coal in boiler converts chemical energy into thermal energy of flue gas which is divided into high, medium and low temperature zones. The heat of flue gas is transferred to CO_2 in the high temperature zone. The main focus of this study is on the absorption of flue gas heat in the middle and low temperature zone.

The thermal efficiency of the S-CO $_2$ cycle will be increased when a multi-stage regenerative heating process is applied. As regeneration performance improves, the flue gas residual heat in the tail flue becomes more difficult to absorb. At present, the FGC method is the most widely used method. A portion of CO $_2$ flow rate is extracted into FGC in the S-CO $_2$ cycle (for example, from a compressor outlet), and heated by residual flue gas heat, then mixes with the main CO $_2$ stream of the cycle (Wang et al., 2021). However, the introduction of new components inevitably leads to increased complexity in the cycle.

Fig. 2 shows the three possible ways to integrate FGC with cycle: LFGC (red heater): a portion of CO_2 flow rate is extracted from

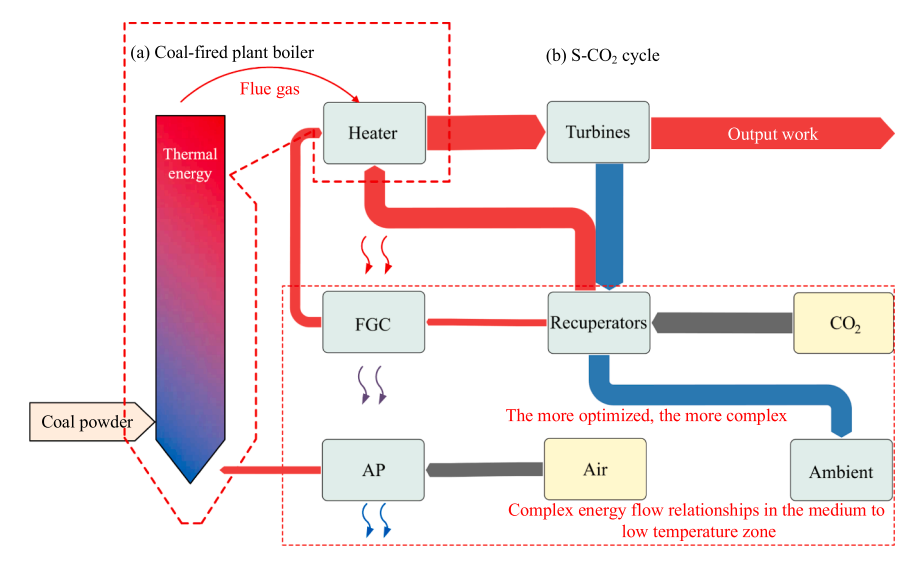


Fig. 1. Energy transfer diagram of coal-fired plant.

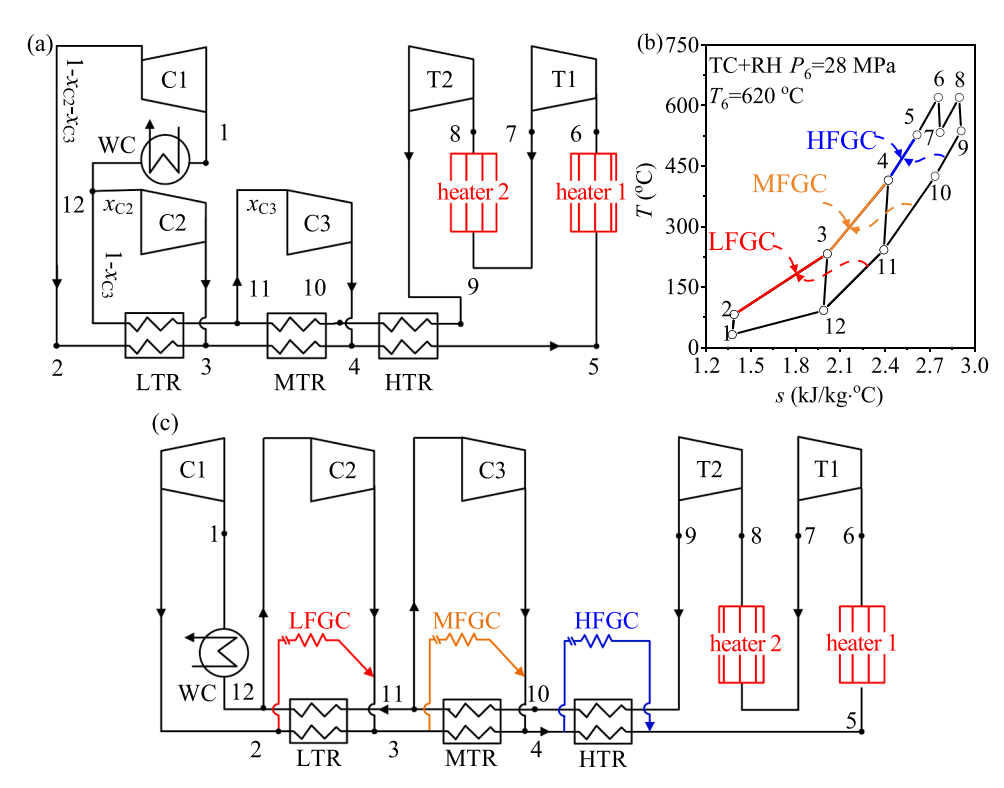


Fig. 2. Three modes for flue gas heat exaction (a: the diagram of TC+RH, b/c: T-s and cycle diagram of coal fired power generation system with three FGC).

compressor C1 outlet, and heated in the LFGC, and heated MTR.

MFGC (yellow heater): a portion of ${\rm CO_2}$ flow rate is extracted from C2 outlet, and heated in the MFGC, then enters HTR.

HFGC (blue heater): a portion of ${\rm CO_2}$ flow rate is extracted from C3 outlet, and heated in the HFGC, then enters heater 1.

Although FGC can solve the problem of the residual flue gas heat absorption, its effect on cycle efficiency is still difficult to understand. For example, (Zhang et al., 2018) believed that the HFGC method has the best effect on improving the cycle thermal efficiency. (Park et al., 2018) argued the LFGC method is the best option, which can improve the net power generation efficiency by 0.15 %. (Mecheri and Le Moullec, 2016) believes that using both LFGC and HFGC methods is more appropriate. For this condition, LFGC, MFGC, and HFGC are applied to absorb flue gas residual heat, respectively. Based on the split method,

the effects evaluation of the FGC becomes the efficiency evaluation of the new adding sub-cycle.

2.2. Research assumptions

The main design parameters of the system were listed in Table 1. The major assumptions were summarized as follows:

- (1) Physical properties of CO₂ come from the REFPROP, which is widely used for cycle analysis (Ruiz-Casanova et al., 2020);
- (2) Mixing flows that have different temperatures and pressures will create irreversibility. Therefore, the following calculations are based on equal temperature and pressure of mixing flows;

Table 1
Parameters for the cycle computation and boiler design (Biencinto et al., 2021; Le Moullec, 2013; Liu et al., 2020).

Parameters	values	unit
Inlet temperature of T1 (T_6)	620	°C
Inlet pressure of T1 (P_6)	28	MPa
Net electrical work (W_{net})	300	MW
Inlet temperature of C1 (T_1)	32	°C
Inlet pressure of C1 (P_1)	7.6	MPa
Turbines isentropic efficiency ($\eta_{T,s}$)	91	%
Compressors isentropic efficiency ($\eta_{C,s}$)	88	%
Pressure drop in regenerator (ΔP)	0.1	MPa
Pinch temperature difference in regenerator ($\Delta T_{\rm pin}$)	10	°C
Pinch temperature difference in cooler ($\Delta T_{\text{pin,cooler}}$)	5	°C
Pinch temperature difference between flue gas and CO_2 ($\Delta T_{pin,b}$)	30	°C
Primary air temperature entering AP ($T_{pri air,in}$)	30	°C
Primary air temperature leaving AP ($T_{pri air}$)	320	°C
Ratio of primary air flow rate to the total air flow rate	19	%
Secondary air temperature entering air preheater ($T_{\text{sec air,in}}$)	25	°C
Ratio of secondary air flow rate to the total air flow rate	81	%
Excess air coefficient (α)	1.2	
Exhaust flue gas temperature ($T_{fg,ex}$)	123.5	°C
Environment temperature (T_0)	24	°C
Pipeline efficiency (η_p)	99	%

- (3) The thermodynamic calculation of the system is based on the energy conservation of each component;
- (4) Except for the cooler, the heat loss of other components shall be ignored (Al-Sulaiman and Atif, 2015; Hou et al., 2017; Sarkar, 2009).

2.3. Analytical model of TC+RH

Fig. 2a deals with the TC+RH by using three compressors (C1-3), a high-temperature recuperator (HTR), a moderate temperature recuperator (MTR), a low-temperature recuperator (LTR), and two turbines (T1-2). Heat was added to the system via heater 1 and heater 2. As the final heat sink, the wet cooler released heat to the environment.

As shown in Fig. 2, the total CO_2 flow rate at the outlet of low-pressure side of MTR (point 11) was split into two parts, with one part flowing through LTR, and the other part flowing through C3. The flow rate entering C3 was x_{C3} , where x_{C3} was called the split ratio of the flow rate. x_{C3} was calculated by the energy conservation across the two sides of MTR:

$$(1 - \mathbf{x}_{C3})(h_4 - h_3) = h_{10} - h_{11} \tag{1}$$

In this study, the split ratios of the flow rate for other compressors were also calculated in a similar way as above. The enthalpy at C1 outlet (point 2) can be calculated by the enthalpy at C1 inlet (point 1) and the isentropic efficiency of compressors (Alsagri et al., 2024; Fallah et al., 2022):

$$\eta_{C,s} = \frac{h_{2,s} - h_1}{h_2 - h_1} \tag{2}$$

Where h is the enthalpy; η is the efficiency; The subscript C indicates compressor, and s indicates isentropic.

The power consumption per unit mass of working fluid flowing through C3 $w_{\rm C3}$ is:

$$w_{\rm C3} = h_4 - h_{11} \tag{3}$$

The enthalpy at T1 outlet (point 7) can be calculated by the enthalpy at T1 inlet (point 6) and the isentropic efficiency of turbines $\eta_{T,s}$ (Fan et al., 2020):

$$\eta_{T,s} = \frac{h_6 - h_7}{h_6 - h_{7,s}} \tag{4}$$

where the subscript T indicates turbine. The output work of unit mass

working fluid flowing through T1 and T2 w_T is:

$$w_{\rm T} = w_{\rm T1} + w_{\rm T2} = h_6 - h_7 + h_8 - h_9 \tag{5}$$

The pinch temperature criterion for recuperators satisfies that (Chen et al., 2020):

$$T_{12} = T_2 + \Delta T_{\text{pin}}, T_{11} = T_3 + \Delta T_{\text{pin}}, T_{10} = T_4 + \Delta T_{\text{pin}}$$
 (6)

Where T means temperature.

Thermal efficiency η_{th} is (Olumayegun et al., 2019):

$$\eta_{\rm th} = 1 - \frac{Q_{\rm r}}{Q_{\rm a}} = \frac{W_{\rm net}}{Q_{\rm a}} \tag{7}$$

where subscripts r and a mean release and absorption, respectively; W_{net} is net power output.

When the $S\text{-}CO_2$ cycle is coupled with the boiler, the thermodynamic calculation of the components in boiler is based on the energy conservation equation:

$$Q_{\rm f} \left(1 - rac{\sum\limits_{
m i=2}^{6} q_{
m i}}{100}
ight) + Q_{
m ap} = Q_{
m a} + Q_{
m ap}$$
 (8)

Where subscript ap means air preheater; q_i means the heat loss (see Table 2 for its specific value). The heat loss of exhaust flue gas (q_2) is:

$$q_2 = \left(\frac{100 - q_4}{100}\right) \frac{h_{\text{fg,ex}} - \alpha h_0}{Q_{\text{f}}} \tag{9}$$

Where $h_{\rm fg,ex}$ and h_0 mean the enthalpy of exhaust flue gas and the air enthalpy at ambient temperature; $Q_{\rm f}$ is the lower heating value of coal (see Table 1 for its specific value). The coal consumption rate $m_{\rm coal}$ is (Dostál, 2004):

$$m_{\rm coal} = \frac{Q_{\rm a}}{\eta_{\rm b} Q_{\rm f}} \tag{10}$$

Where η_b is boiler efficiency, which can be calculated according to the anti-balance method:

$$\eta_{\rm b} = 1 - \frac{\sum_{\rm i=2}^{6} q_{\rm i}}{100} \tag{11}$$

The net power generation efficiency η_e is:

$$\eta_{\rm e} = \eta_{\rm b} \eta_{\rm th} \eta_{\rm p} \tag{12}$$

Where η_p is the pipeline efficiency, and the specific value is shown in Table 1.

2.4. 2.4 The exergy analyses

Table 3 (Liu et al., 2020) presents the equations for cycle parameters at distinct state points. The specific exergy per unit mass flow rate can be calculated using the formula $e = h - T_0 s$, where s denotes the entropy value of the working fluid per unit mass flow rate. The exergy loss is determined by the difference between the input and output exergy values.

Exergy efficiency η_{ex} is defined as:

$$\eta_{\rm ex} = \frac{W_{\rm net}}{E_{\rm in}} \tag{13}$$

Table 2 Various heat losses of boiler(%) (Boiler exhaust temperature is 123°C).

q_4	q_3	q_2	q_5	q_6	$\eta_{ m b}$
1.60	0.00	4.77	0.40	0.30	92.93

Table 3 Equations for components in the cycle (Liu et al., 2020).

Equations and exergy destructions Components $\eta_{\text{C,s}} = \frac{h_{2,s} - h_1}{h_2 - h_1}, \quad w_{\text{Cl}} = (1 - x_{\text{C2}})(h_2 - h_1);$ $i_{C1} = w_{C1} - (1 - x_{C2})(e_2 - e_1)$ $\eta_{\text{C,s}} = \frac{h_{3,s} - h_{12}}{h_3 - h_{12}}, \quad w_{\text{C2}} = x_{\text{C2}}(h_3 - h_{12});$ $i_{C2} = w_{C2} - x_{C2}(e_3 - e_{12})$ $\eta_{\text{C,s}} = \frac{h_{4,s} - h_{11}}{h_4 - h_{11}}, \ W_{\text{C3}} = X_{\text{C3}}(h_4 - h_{11});$ $i_{C3} = w_{C3} - x_{C3}(e_4 - e_{11})$ $\eta_{\text{T,s}} = \frac{h_6 - h_7}{h_{6,s} - h_7}, \quad w_{\text{T1}} = h_6 - h_7, \quad i_{\text{T1}} = e_6 - e_7 - w_{\text{T1}}$ $P_8 = \sqrt{P_6 P_9}$, $\eta_{T,s} = \frac{h_8 - h_9}{h_{8,s} - h_9}$, $w_{T2} = h_8 - h_9$; $T_{11} = T_3 + \Delta T_{\text{pin}}$, $i_{\text{MTR}} = e_{10} - e_{11} - (1 - x_{\text{C3}} - x_{\text{MFGC}})(e_4 - e_3)$ 11 10 3 MTD 4 $i_{\text{HTR}} = e_9 - e_{10} - (1 - x_{\text{HFGC}})(e_5 - e_4)$ $i_{\text{Ccooler}} = (1 - x_{\text{C3}} - x_{\text{C2}})(e_{10} - e_{1})$

The input exergy of the system can be compared to the chemical exergy of coal (Hanak et al., 2020):

$$E_{\rm in} = m_{\rm coal} Q_{\rm LCV} \left(1.0064 + 0.1519 \frac{H_{\rm ar}}{C_{\rm ar}} + 0.0616 \frac{O_{\rm ar}}{C_{\rm ar}} + 0.0429 \frac{N_{\rm ar}}{C_{\rm ar}} \right) \quad (14)$$

The boiler exergy loss $I_{\rm b}$ is defined as:

$$I_{\rm b} = E_{\rm in} - E_{\rm b} \tag{15}$$

The boiler output exergy is equivalent to the S-CO2 cycle input

exergy

$$E_{\rm b} = m_{\rm CO2}(e_5 - e_4 + e_7 - e_6) + m_{\rm FGC}(e_{\rm FGC,out} - e_{\rm FGC,in})$$
 (16)

The exergy balance of each component can be expressed as (Arslan, 2021; Arslan and Erbas, 2021):

$$E_{k}^{Q} - E^{W} + \sum (m_{in}e_{in})_{k} - \sum (m_{out}e_{out})_{k} = I_{k}$$
 (17)

Where the subscript k represents the k-th component, and E_k^Q, E_k^W, e_k, I_k

respectively means the heat exergy, work exergy, the specific exergy of working fluid, and the exergy loss. E_k^Q can be calculated as follows (Erikgenoğlu and Arslan, 2024):

$$E_{\mathbf{k}}^{Q} = \left(1 - \frac{T_0}{T}\right) Q_{\mathbf{k}} \tag{18}$$

$$Q_{k} = W_{k} + (m_{\text{out}}h_{\text{out}})_{k} - (m_{\text{in}}h_{\text{in}})_{k}$$
(19)

The specific calculation formulas for e_k are listed in Table 3, and E_k^W can be calculated as follows:

$$E_{k}^{W} = W_{k} \tag{20}$$

2.5. Model validation

The S-CO $_2$ coal-fired power generation is still an emerging thermal energy conversion technology. Although some experimental studies have been conducted, the majority of research primarily relies on thermodynamic simulation method (Feher, 1968; Le Moullec, 2013; Mecheri and Le Moullec, 2016; Wu et al., 2020), and the first law of thermodynamics is strictly followed. The simulation results from (Zhang et al., 2018) are used to validate the method in this study. Table 4 lists the main design parameters from the reference, and Table 5 presents the comparison results. The error ranges from 0.02 % to 1.48 %, indicating that the calculated data align well with the literature results.

3. Applying the split method to analyze coal-fired power generation systems with FGC

3.1. The essence of the splitting method

The split method is an effective tool for analyzing complex systems. As shown in Fig. 3, in order to meet higher demands, additional components need to be added to the conventional system A. This means that the system will tend to become more complex (complicated system B), and the characteristics of the system construction process are difficult to understand. By applying the split method, system B can be equated to system A with the addition of a new system C. Consequently, the analysis of the complex system B can be considered equivalent to the analysis of the added system C. The reasons for inefficiency or efficiency can be identified more easily.

3.2. Case 1: the effect of LFGC on coal-fired power generation system

Fig. 4a shows the TC+RH coal-fired power generation system with LFGC, recorded as TC+RH+LFGC. Compared to the TC+RH, an LFGC is arranged in the boiler flue duct to absorb residual heat. Based on the content of Section 3.1, we prefer to split the LFGC in to a new sub-cycle, which will simplify the complexity of the system analysis. Based on this idea, we apply the split method to decouple the LFGC from the system,

Table 4
Main parameters (Zhang et al., 2018).

Parameters	values	Unit
High pressure turbine inlet temperature	600.0	°C
High pressure turbine inlet pressure	31.0	MPa
High pressure turbine outlet temperature	508.1	°C
High pressure turbine outlet pressure	15.5	MPa
Low pressure turbine inlet temperature	620.0	°C
Low pressure turbine outlet temperature	529.3	°C
Main compressor inlet temperature	32	°C
Main compressor inlet pressure	7.6	MPa
Pressure drops (every component)	0.1	MPa
LTR and HTR pinch	5	°C
Compressor efficiency	90	%
Net capacity	1000	MWe
Boiler discharge temperature	264.0	°C

Table 5Comparison of the calculation results and the reference data.

Parameters	Ref data (Zhang et al., 2018)	Calculation results	error
T ₂ (°C)	82.1	82.5	0.49 %
T ₃ (°C)	226.8	226.9	0.04 %
T ₄ (°C)	489.1	489.0	-0.02~%
T ₉ (°C)	231.8	231.9	0.04 %
T ₁₀ (°C)	87.1	87.5	0.46 %
split ratio (%)	32.6 %	32.5 %	-0.31 %
Power consumption of MC (MW)	222.24	220.55	-0.76 %
Power consumption of RC (MW)	171.69	174.23	1.48 %
heat transfer load of cooler (MW)	853.69	853.52	-0.02 %
Turbine power (MW)	1393.92	1394.78	0.06 %
Net efficiency (%)	45.96	45.97	0.02 %

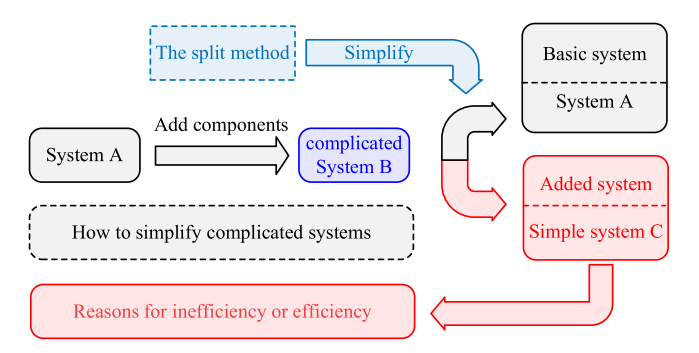


Fig. 3. The split method can simplify the difficulty of analyzing complicated systems.

and the 12–1–2–3 thermodynamic process are separated from TC+RH+LFGC. Accordingly, a reverse compression process (Δh_{3-12}) is added to the thermodynamic process of 12–1–2–3, that is, the CO₂ flow rate at the C2b inlet (point 12) returns to the C2b outlet (point 3). Then, the thermodynamic process 3–12–1–2–3 (see Fig. 4c) can be regarded as a simple regenerative cycle (SC). Therefore, TC+RH+LFGC can be equivalent to adding a SC to TC+RH (see Fig. 4).

It is worth noting that the inverse compression process in SC is virtual and is designed to offset the effect of increasing the $\rm CO_2$ flow rate at the C2a inlet in TC+RH. If SC and TC+RH are considered separately, it will lack definite physical meaning. The splitting process of the cycle is reversible, that is, some components with similar pressure/temperature values among the two sub-cycles can be shared and combined to form TC+RH+LFGC. This is in line with the characteristics of the split method. The thermal efficiency of TC+RH+LFGC formed by superposition of SC and TC+RH will decrease because the equivalent turbine inlet temperature of SC (T_3) is much lower than that of TC+RH (T_6). This conclusion can also be proved by theoretical derivation.

The net power output $W_{\mathrm{net,TR}}$ and heat absorption $Q_{\mathrm{a,TR}}$ of TC+RH are:

$$Q_{a,TR} = m_{CO2,TR} (h_6 - h_5 + h_8 - h_7)$$
(17)

$$W_{\text{net,TR}} = m_{\text{CO2,TR}} (w_{\text{T1}} + w_{\text{T2}} - x_{\text{C1}} w_{\text{C1}} - x_{\text{C2}} w_{\text{C2}} - x_{\text{C3}} w_{\text{C3}})$$
(18)

Where subscript TR means TC+RH. Combining Eqs. (17) and (18), the cycle thermal efficiency $\eta_{th,STR}$ is:

$$\eta_{\text{th,TR}} = \frac{W_{\text{net,TR}}}{Q_{\text{a,TR}}} = \frac{(w_{\text{T1}} + w_{\text{T2}} - x_{\text{C1}}w_{\text{C1}} - x_{\text{C2}}w_{\text{C2}} - x_{\text{C3}}w_{\text{C3}})}{(h_6 - h_5 + h_8 - h_7)}$$
(19)

For SC, the net power output $W_{\rm net,SC}$ and heat absorption $Q_{\rm a,SC}$ are:

$$Q_{a,SC} = Q_{LFGC} = m_{CO2,SC}(h_3 - h_2)$$
 (20)

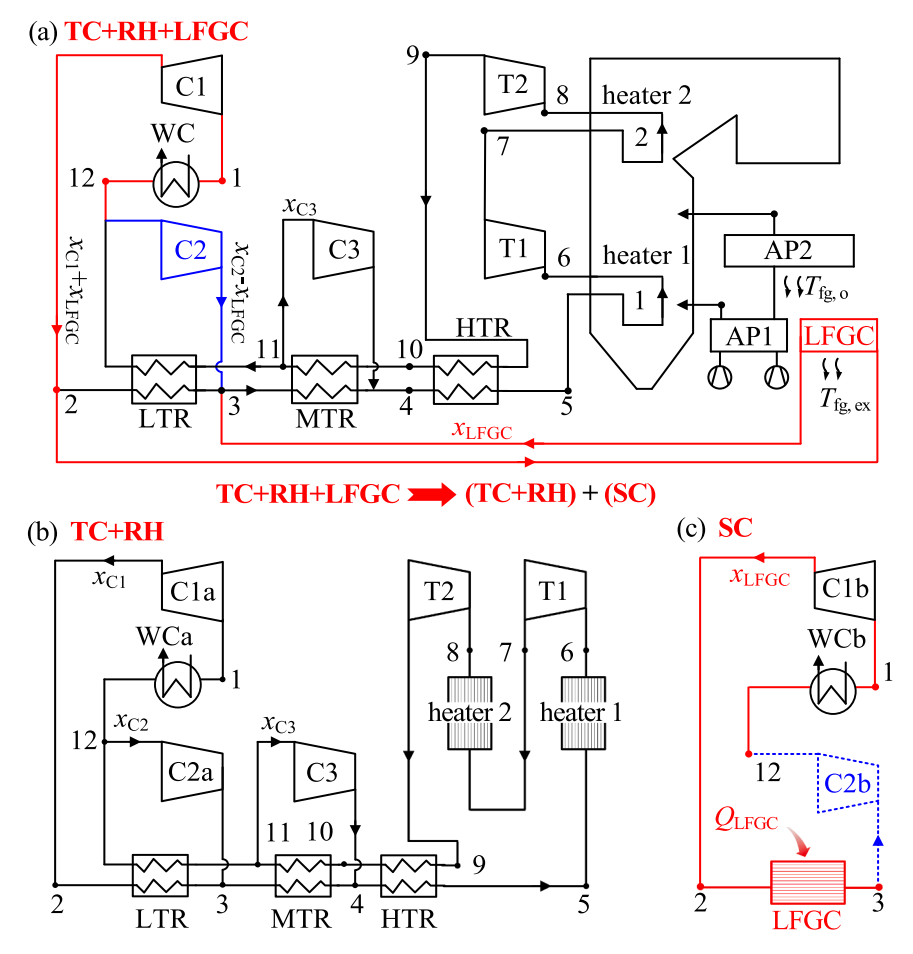


Fig. 4. The split diagram for TC+RH+LFGC.

$$W_{\text{net,SC}} = m_{\text{CO2,SC}} \left(w_{\text{C2}} - w_{\text{C1}} \right) \tag{2}$$

Combining Eqs. (20) and (21), the cycle thermal efficiency $\eta_{th,SC}$ is:

$$\eta_{\text{th,SC}} = \frac{W_{\text{net,SC}}}{Q_{\text{a,SC}}} = \frac{m_{\text{CO2,SC}}(w_{\text{C2}} - w_{\text{C1}})}{Q_{\text{LFGC}}} = \frac{w_{\text{C2}} - w_{\text{C1}}}{h_3 - h_2}$$
(22)

According to Eq. (22), the value of $\eta_{th,SC}$ is only related to the parameters of the cycle state points, thus $\eta_{th,SC}$ remains constant. Then, the thermal efficiency of TC+RH+LFGC η_{th} is:

$$\eta_{\rm th} = \frac{W_{\rm net,TR} + W_{\rm net,SC}}{Q_{\rm a,TR} + Q_{\rm a,SC}} \tag{23}$$

Eq. (23) is modified as:

$$\eta_{\text{th}} = \frac{\eta_{\text{th,TR}} Q_{\text{a,TR}} + \eta_{\text{th,SC}} Q_{\text{a,SC}}}{Q_{\text{a,TR}} + Q_{\text{a,SC}}} = \eta_{\text{th,TR}} + \frac{(\eta_{\text{th,SC}} - \eta_{\text{th,TR}}) Q_{\text{a,SC}}}{Q_{\text{a,TR}} + Q_{\text{a,SC}}}$$
(24)

From Eq. (21), when $\eta_{\text{th,SC}} < \eta_{\text{th,TR}}$, η_{th} will decrease. Fig. 5 shows the *T-s* diagram of split cycles. With $T_6 = 620\,^{\circ}\text{C}$ and $P_6 = 28\,\text{MPa}$, the thermal efficiency $\eta_{\text{th,TR}}$ keeps 51.38 % for TC+RH. The thermal

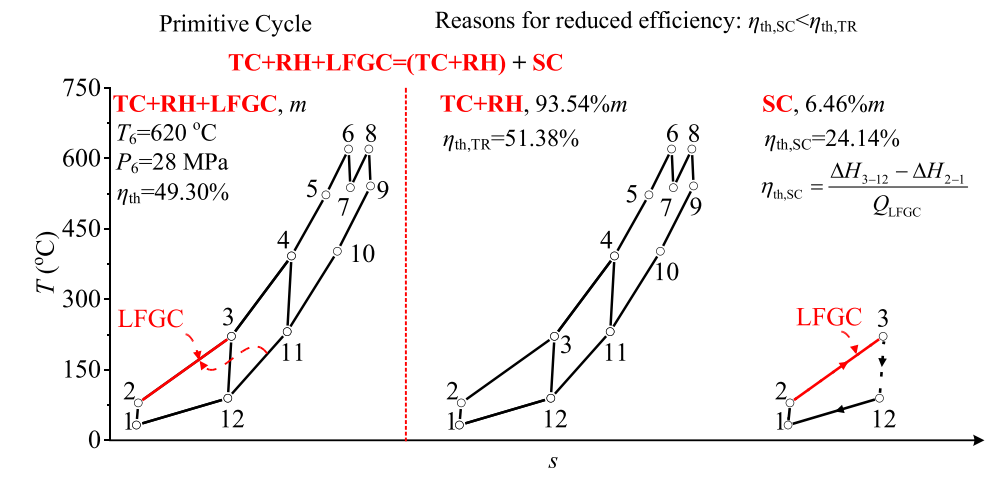


Fig. 5. Case 1: the relationship between TC+RH+LFGC and its two subsystems of TC+RH and SC.

efficiency of SC $\eta_{th,SC}$ is 24.14 %, thus the thermal efficiency of TC+RH+LFGC η_{th} is 49.94 %. Results are consistent with the theoretical derivation. In summary, the split method shows that TC+RH+LFGC can be equivalent to adding a new sub-cycle with lower efficiency to TC+RH, and then the thermal efficiency for TC+RH+LFGC will be decreased.

3.3. Case 2: the effect of MFGC on coal fired power generation system

MFGC and LFGC have the same principle. Part of the CO_2 flow rate at the C3 inlet is flowed into the MFGC to absorb the residual flue gas heat. Similarly, based on the CO_2 flow rate at the MFGC inlet, we split TC+RH+MFGC to obtain a C1a/2a/3a split ratio of $x_{\rm C1}/x_{\rm C2}/x_{\rm C3}$ for sub-TC+RH by increasing the CO_2 flow rate at the C3a inlet. Accordingly, a reverse compression process (Δh_{4-11}) is added, and then a virtual RC is obtained (see Fig. 6).

The heat absorption $Q_{a,RC}$ for sub-RC+MFGC is:

$$Q_{a,RC} = Q_{MFGC} = m_{CO2,RC}(h_4 - h_3)$$
 (25)

Then, the split ratio of x_{C2b} is:

$$x_{\rm C2b} = 1 - \frac{h_{11} - h_{12}}{h_3 - h_2} \tag{26}$$

The net power output $W_{\text{net,RC}}$ is:

$$W_{\text{net,RC}} = m_{\text{CO2,RC}} \left[w_{\text{C3}} - x_{\text{C2b}} w_{\text{C2}} - (1 - x_{\text{C2b}}) w_{\text{C1}} \right]$$
 (27)

The thermal efficiency of RC $\eta_{th,RC}$ is:

$$\eta_{\text{th,RC}} = \frac{W_{\text{net,RC}}}{Q_{\text{a,RC}}} = \frac{w_{\text{C3}} - x_{\text{C2b}}w_{\text{C2}} - (1 - x_{\text{C2b}})w_{\text{C1}}}{h_4 - h_3}$$
(28)

Similarly, the value of $\eta_{\rm th,RC}$ is only related to the parameters of the cycle state points. Fig. 6 shows the *T-s* diagram and calculation results of the split cycles with $T_6=620~{\rm ^{\circ}C}$ and $P_6=28$ MPa. TC+RH+MFGC can be equivalent to adding a new sub cycle with 43.77 % efficiency to TC+RH. Compared with LFGC, the thermal efficiency for RC is higher than that for SC (from 24.14 % to 43.77 %), but it is still lower than TC+RH thermal efficiency (51.38–50.86 %). Therefore, the cycle thermal efficiency is still decreased by applying MFGC.

3.4. Case 3: the effect of HFGC on coal-fired power generation system

Fig. 7 shows the T-s diagram and calculation results of the split cycles. The thermal process formed by CO_2 flow rate at the FGC inlet is TC2 +RH, then the heat released from the 9–10 process will go to TC+RH. The remaining working fluid forms TC+RH. The split ratio of the working fluid entering compressors in new sub-cycle is the same as

TC+RH. As shown in Fig. 7, the regenerative heat transfer of the two subcycles is the same under the unit mass flow. Since the turbine inlet temperature and the cooler inlet temperature are equal for two subcycles, the heat absorption and heat released are also equal with the unit mass flow. Therefore, the thermal efficiency of TC2 +RH is equal to that of TC+RH. In other words, TC+RH+HFGC can be equivalent to adding a new subcycle with the same efficiency (51.38 %) to TC+RH. Then the thermal efficiency of TC+RH+HFGC remains constant.

According to the energy conservation of HTR in Fig. 7b, h_9 - h_{10} = h_5 - h_4 . Then, the heat absorption $Q_{\rm HFGC}$ for HFGC is:

$$Q_{\rm HFGC} = m_{\rm CO2,TR2} \left(h_5 - h_4 \right) \tag{29}$$

The thermal efficiency $\eta_{\text{th,TR2}}$ for TC2 +RH is:

$$\eta_{\text{th,TR2}} = \frac{W_{\text{net,TR2}}}{Q_{\text{a,TR2}}} = \frac{m_{\text{CO2,TR2}} \left(w_{\text{T1}} + w_{\text{T2}} - x_{\text{C1}} w_{\text{C1}} - x_{\text{C2}} w_{\text{C2}} - x_{\text{C3}} w_{\text{C3}} \right)}{m_{\text{CO2,TR2}} \left(h_6 - h_{5''} + h_8 - h_7 \right) + Q_{\text{HFGC}}}$$
(30)

From Eq. (29), Eq. (30) can be modified as:

$$\eta_{\text{th,TR2}} = \frac{m_{\text{CO2,TR2}} (w_{\text{T1}} + w_{\text{T2}} - x_{\text{C1}} w_{\text{C1}} - x_{\text{C2}} w_{\text{C2}} - x_{\text{C3}} w_{\text{C3}})}{m_{\text{CO2,TR2}} (h_6 - h_5 + h_8 - h_7)} = \eta_{\text{th,TR2}}$$
(31)

This mathematical derivation is congruent with thermodynamic calculations (see Fig. 7). This result means that coupling HFGC will increase the temperature at point 5 of the system, while the total heat absorption of the system remains constant, and the heat absorption temperature zone is extended. Consequently, the system with HFGC has the ability to absorb residual flue gas heat without any reduction efficiency.

Through the split method, the performance evaluation of the complex cycle can be equivalent to the thermodynamic performance evaluation of sub-cycles. Applying the split method shows that, the new sub-cycle thermal efficiency is not better than TC+RH. This conclusion explains the decrease in cycle thermal efficiency after coupling LFGC or MFGC. By splitting the cycle, the optimized path becomes more clearly, that is, to improve the new sub-cycle thermal efficiency. Then, we will provide a new optimization method in the next section.

4. Cycle optimization based on split method

Fig. 8 shows the roadmap for the split method to analysis cycle performance. In Section 3, the effect of the FGC is explained more clearly. Further, after coupling the FGC, the reason for the reduced efficiency is found by applying the split method, that is a new inefficient sub-cycle is added to TC+RH. To solve this problem, low-grade heat was converted into high-grade heat for heating the new sub-cycle. Then, the

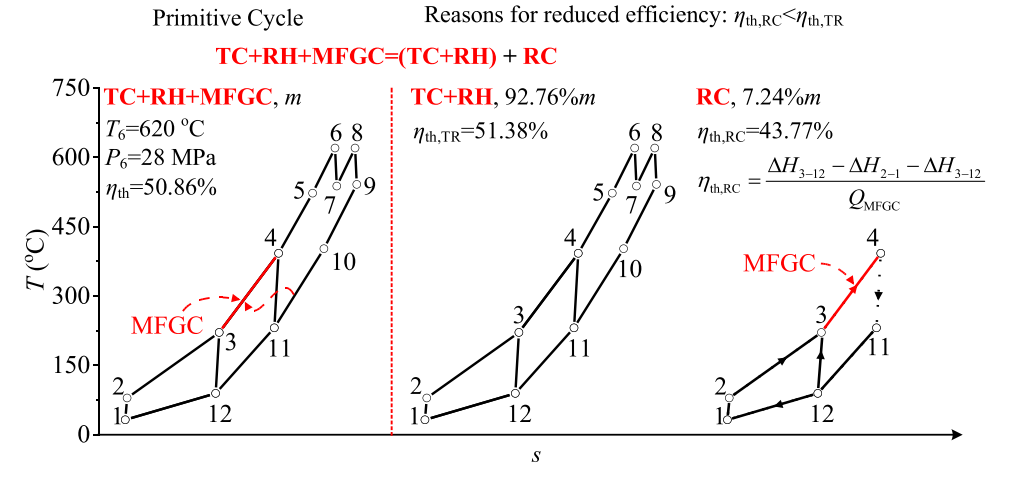


Fig. 6. Case 2: The relationship between TC+RH+MFGC and its two subsystems of TC+RH and RC.

Primitive Cycle Reasons for constant efficiency: $\eta_{\text{th,TC2}} = \eta_{\text{th,TR}}$

Fig. 7. Case 3: the relationship between TC+RH+HFGC and its two subsystems of TC+RH and TC2+RH.

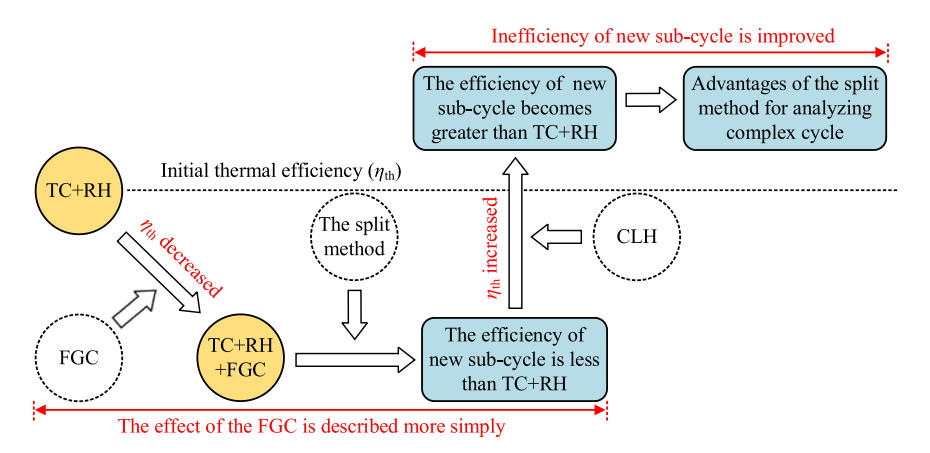


Fig. 8. the roadmap for the split method to analysis cycle performance.

stepwise optimization scheme of Case A-C is proposed, and the thermal efficiency is improved.

4.1. Case A: TC+RH+ LFGC coupled with the CLH method

Fig. 9 is the schematic diagram of the CLH method. The characteristic of heat released process in S-CO $_2$ cycle with variable temperature can be utilized (Liu et al., 2019; Tong et al., 2022), then the residual heat of dry-cooler is recovered to boiler. For maintaining the boiler efficiency, the additional flue gas heat was used for heating the new sub-cycle. Therefore, it can be considered that some of the waste heat from the dry-cooler is used to heat the new sub-cycle. Then, the thermal efficiency is improved.

Here we apply the split method to the analyses of TC+RH+LFGC. As shown in Fig. 10, when the CLH method is coupled to the system, part of the heat released from the cycle to the environment is recovered to the boiler via air. At this moment, the cooler heat recovery Q_{re} is:

$$Q_{\rm re} = x_{\rm C1} m_{\rm CO2} (h_{12} - h_{\rm a}) \tag{32}$$

The air temperature at the inlet of AP $(T_{air.in})$ is:

$$T_{\rm air,in} = T_{12} - \Delta T_{\rm pin,cooler} \tag{33}$$

TC+RH+LFGC can be split into the TC+RH and SC. The heat absorption $Q_{\rm a,SC}$ for SC is $Q_{\rm LFGC}$ - $Q_{\rm re}$, and this means that the thermal efficiency of the SC can be improved. Then the thermal efficiency for TC+RH+LFGC $\eta_{\rm th}$ will be increased. The formula for $\eta_{\rm th}$ is derived as follows:

$$\eta_{\rm th} = \frac{W_{\rm net,TR} + W_{\rm net,SC}}{Q_{\rm a,TR} + Q_{\rm a,SC}} = \frac{W_{\rm net,TR} + W_{\rm net,SC}}{Q_{\rm a,TR} + (Q_{\rm LFGC} - Q_{\rm re})}$$
(34)

With $T_6=620~^\circ$ C and $P_6=28$ MPa, when $\eta_{th,TR}$ is 51.38 %, the $\eta_{th,SC}$ increases from 24.14 % to 33.12 %. Therefore, the thermal efficiency of TC+RH+LFGC increases from 49.30 % to 49.77 %, which is consistent with the derivation of formulas.

4.2. Case B: TC+RH+M/LFGC coupled with the CLH method

In case A, the introduction of the CLH method makes the efficiency of the new sub-cycle SC better. Then, we would like to bring this gain to TC+RH+MFGC. It is worth noting that, the application of a single MFGC cannot fully absorb flue gas residual heat. So, LFGC is continued to be applied, and the cycle is changed to TC+RH+M/LFGC. Fig. 11 shows the split *T-s* diagram for TC+RH+M/LFGC. The system can be still considered as adding a RC to TC+RH. When the cooler heat recovery is $Q_{\rm re}$, the heat absorption of RC ($Q_{\rm a,RC}$) is $Q_{\rm MFGC}+Q_{\rm LFGC}-Q_{\rm re}$. The calculations show that the thermal efficiency of RC increases from 43.77 % to 58.43 %, and then the thermal efficiency of the whole cycle increases from 50.86 % to 51.87 %. Apparently, the optimized pathway to improve the thermal efficiency of the new sub-cycle is proved again.

4.3. Case C: TC+RH+FGC coupled with the CLH method

Similar to Case B, a single HFGC cannot absorb the flue gas residual heat from TC+RH+HFGC when applying the CLH method. Then, three FGC methods are applied to ensure constant boiler efficiency. Fig. 12 shows the split *T-s* diagram for TC+RH+FGC. To ensure that the split

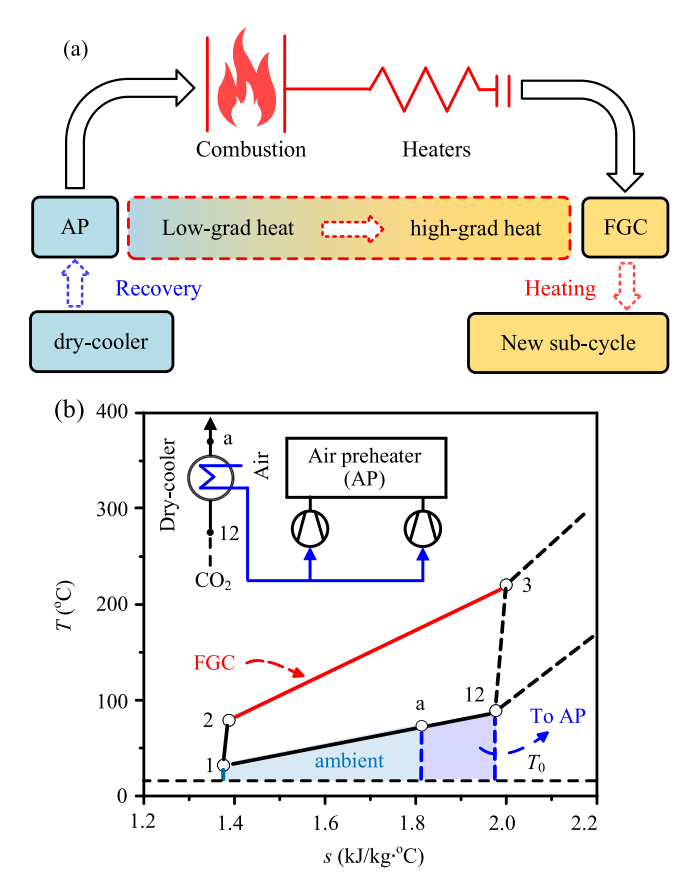


Fig. 9. The new cycle optimization method (a: diagram of the CLH method principle, b: *T*-s diagram of cycle coupled with CLH.

ratio of compressors working fluid in TC+RH remains constant, a reverse compression process (Δh_{4-11}) should be added, that is, the CO₂ flow rate at the C3b inlet (point 11) returns to the C3b outlet (point 4). Therefore, the system can be considered as adding a RC+RH to TC+RH. The results of the cycle splitting show that, the thermal efficiency of RC+RH is 62.38 %, higher than TC+RH (51.38 %). Then, TC+RH+FGC has the best performance with a thermal efficiency of 52.41 %.

Fig. 13 shows the final power generation system. FGC and AP are arranged in parallel in the boiler tail flue. And then, the heat absorption temperature range of air in the AP is increased. Ultimately, it ensures that the residual heat of the flue gas is fully absorbed.

The heat loads for different heat exchangers are given in Fig. 14. The

calculation results shows that although the heat load of the heaters is 528.00 MW, the heat transfer between the flue gas and CO_2 is easy to achieve. The pinch point issue occurs in the low-temperature flue gas area. The introduction of FGC ensures that the minimum heat transfer temperature difference at each heat exchange surface is equal to 30 $^{\circ}$ C, which meets the design values. The heat load for AP+FGC is 141.49 MW.

4.4. Energy and exergy analysis

For making the data of Case C easy to understand, Sankey diagrams are used to describe the flow paths of energy and exergy. The red line represents a flow trend from left to right, while the blue line represents a flow trend from right to left, and the gray lines represent energy or heat losses.

Fig. 15a shows the energy flow diagram of TC+RH+FGC coupled with the CLH method. For turbines, the cycle input energy is divided into two parts. A part of the energy is used to drive the compressor (172.7 MW), while the other part becomes output work (300 MW). For recuperators, the energy flow occurs within the component and there is no heat loss. The heat load of the recuperators is 1287.8 MW, which is four times the output power. For the S-CO₂, there are two parts to the recycle input energy. One is the air recovery heat (15.0 MW), and the other is the flue gas heat released (616.1 MW-43.6 MW). Heat loss also consists of two parts, the one is exhaust flue gas heat (43.6 MW), and the other is heat released from the cooler to the ambient (272.4 MW).

Fig. 15b shows the exergy flow diagram of TC+RH+FGC coupled with the CLH mehtod. The cycle input exergy for chemical exergy is 631.3 MW. Specific values of exergy loss for components are shown in Fig. 15b. The boiler exergy loss is largest, which is 263.3 MW, and the cooler recovery exergy is 0.7 MW. The total exergy loss is 329.3 MW.

The data in the Sankey diagram all satisfy the conservation law of energy and exergy. Results show that, the thermal efficiency is 52.41 %, the exergy efficiency is 47.52 %, and the net power efficiency is 48.23 %. The exergy and thermal efficiency of the different cycles are compared in Fig. 16. In this paper, the split method is first used complex S-CO₂ cycle analysis for coal-fired heat sources, and the inefficiency reason for cycle coupled with FGC is found: a new sub-cycle below the TC+RH efficiency is added. Then, the CLH is introduced, and the efficiency of the new sub-cycle becomes higher than that of TC+RH. The validity of the split method is further proved by thermodynamic calculations.

4.5. Parametric analysis

For the S-CO₂ Brayton cycle, the outlet temperature of the cooler (T_1)

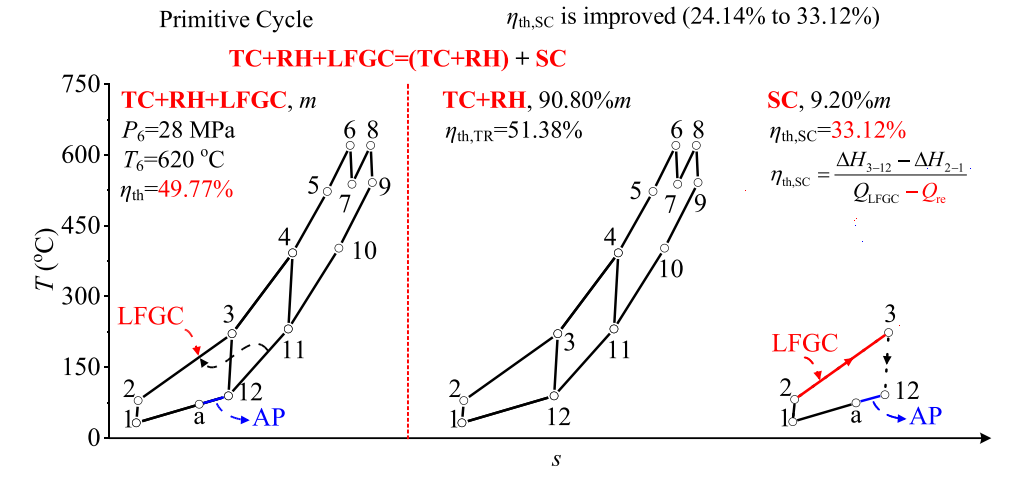


Fig. 10. The relationship between TC+RH+LFGC coupled with the CLH and its two subsystems of TC+RH and SC.

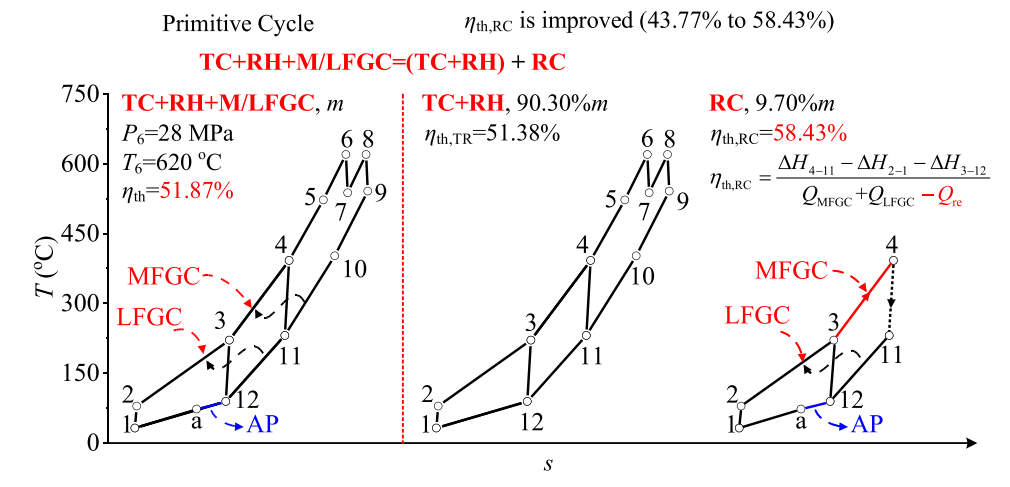


Fig. 11. The relationship between TC+RH+M/LFGC coupled with the CLH and its two subsystems of TC+RH and RC.

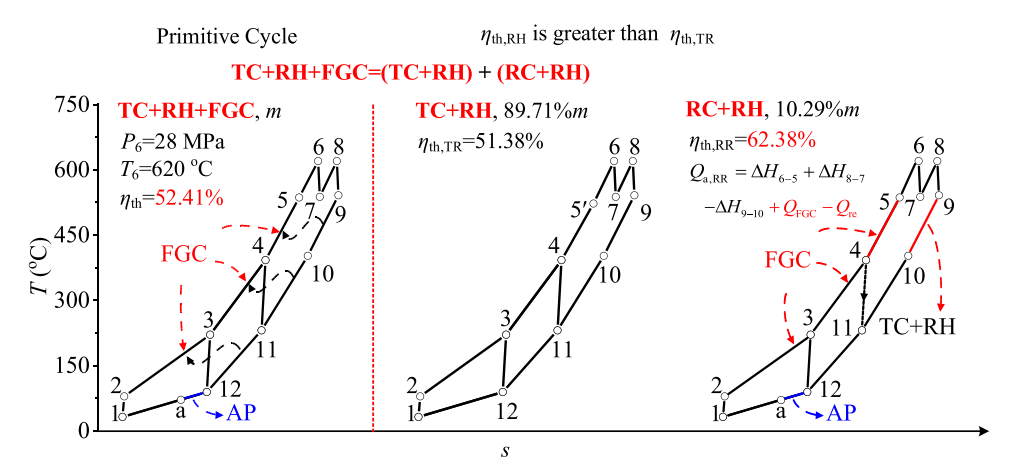
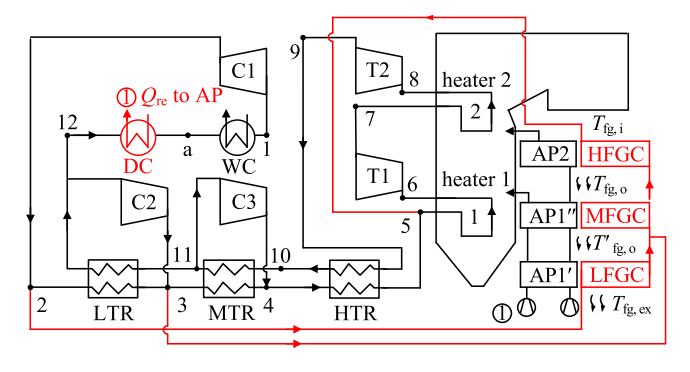


Fig. 12. The relationship between TC+RH+FGC coupled with the CLH and its two subsystems of TC+RH and RC+RH.



 $\textbf{Fig. 13.} \ \ \textbf{TC+RH+FGC} \ \ \textbf{coupled} \ \ \textbf{with} \ \ \textbf{CLH} \ \ \textbf{coal} \ \ \textbf{fired} \ \ \textbf{power} \ \ \textbf{generation} \ \ \textbf{system}.$

is a very important design parameter. We hope it remains at a lower design value to achieve higher thermal efficiency. However, in practical electricity generation processes, the T_1 will increase due to rising environmental temperatures. Will the gains brought by the CLH method be diminished? For answering the question, the impact of T_1 changes on thermal efficiency has been analyzed. As shown in Fig. 17, when the T_1 increases from 32 °C to 37 °C, the thermal efficiency gradually deteriorates. Because the increase in T_1 leads to higher average heat released temperature of the cycle. Then, the recovered waste heat from the air will also increase, thereby amplifying the benefits brought by the CLH method. Therefore, the efficiency gap between the optimized cycle

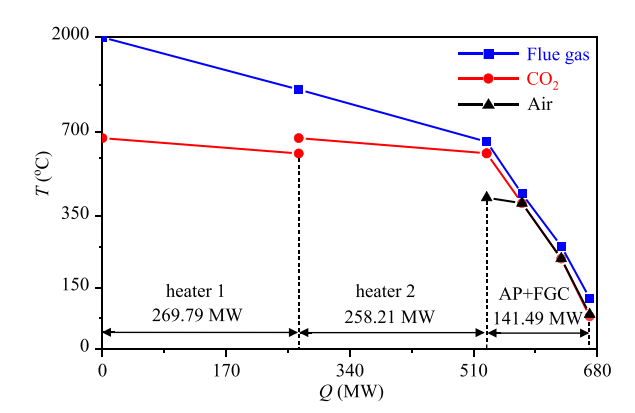


Fig. 14. The heat transfer T-Q diagram in Boiler.

and the unoptimized cycle has increased from 1.03 % to 2.16 %.

5. Conclusions

The S-CO $_2$ coal-fired power generation systems are usually complex and difficult to compare. In this context, the advantages of the split method in analyzing complex coal fired systems are shown in the effect analysis of different FGC methods on TC+RH. Then, the split method inspires us to construct a more efficient cycle by coupling the CLH method. The following conclusions are drawn:

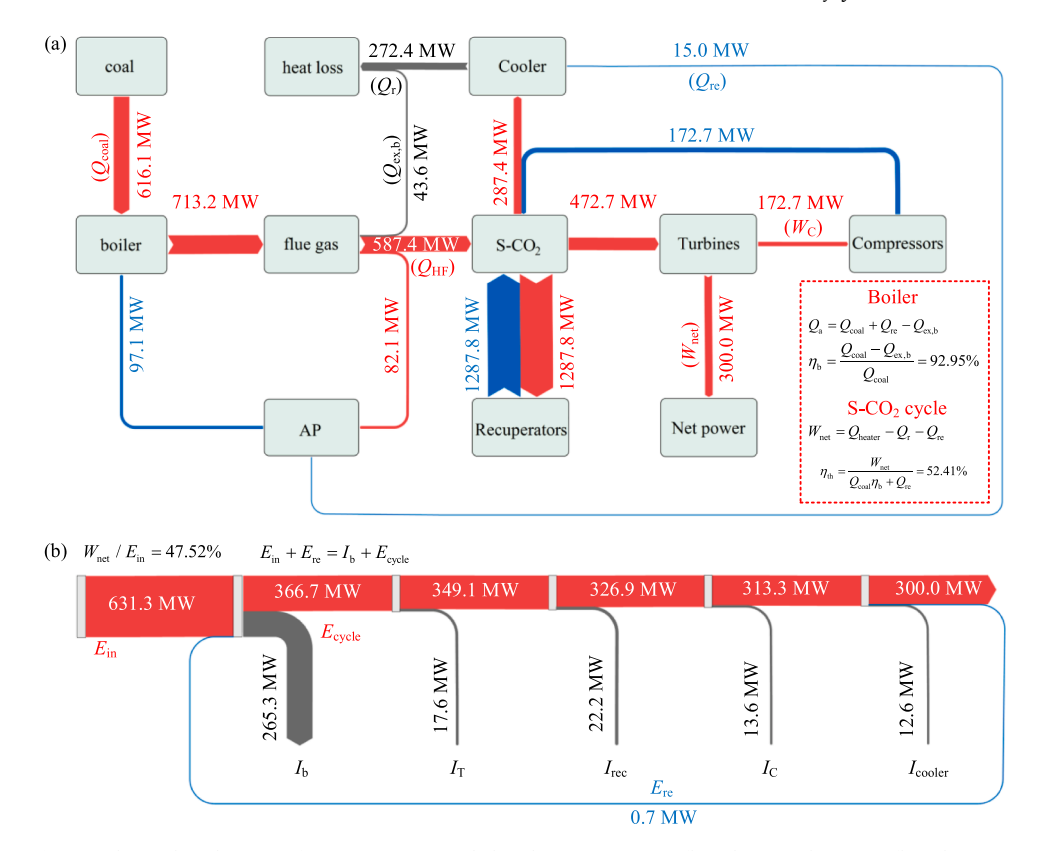


Fig. 15. the Sankey diagram of TC+RH+FGC coupled with CLH (a: energy flow diagram, b: exergy flow diagram).

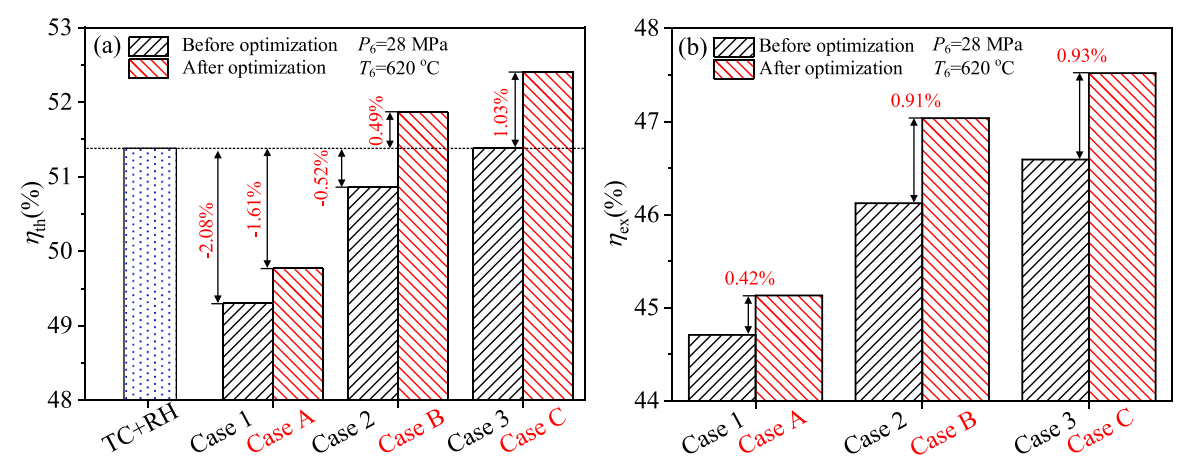


Fig. 16. The cycle Efficiency Comparison (a: thermal efficiency; b: exergy efficiency).

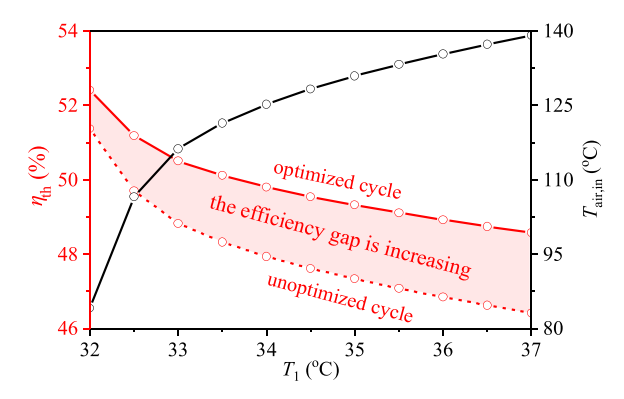


Fig. 17. The impact of T_1 changes on thermal efficiency.

- (1) Using the split method to more clearly reveal the essence of the FGC method. When the FGC is coupled with TC+RH, it does not contribute to improving thermal efficiency. The thermal efficiency of TC+RH+LFGC and TC+RH+MFGC decreased by 2.08 % and 1.61 %, respectively, while TC+RH+HFGC is consistent with the efficiency of TC+RH.
- (2) The CLH method was proposed to improve the thermal efficiency of the new sub-cycle. Finally, the thermal efficiency of optimized cycle has improved from 51.38 % to 52.41 %, and the exergy efficiency reaches 47.52 %.
- (3) The parametric analysis was conducted. When the cooler outlet temperature increases from 32 °C to 37 °C, the efficiency gain from applying the CLH method becomes more significant. The efficiency gap between the optimized cycle and the unoptimized cycle has increased from 1.03 % to 2.16 %.

In this study, the split method is used to simplify the coal-fired S-CO $_2$ cycle, making it easier to optimize performance. This approach can also be applied to integrated energy systems. Modules such as heating, electricity and gas can be divided into different subsystems. The research on collaborative optimization potential of subsystems aims to improve overall energy utilization efficiency and reduce carbon emissions. Additionally, the application fields of the CHL method can also be broadened. The essence of the CHL method lies in the cascade utilization of energy, and it has great potential for optimization in waste heat recovery power plant.

CRediT authorship contribution statement

Guo Yuandong: Writing – review & editing, Writing – original draft, Investigation. Sun Enhui: Writing – review & editing, Methodology. Xu Jinliang: Writing – review & editing, Supervision. Chang Cheng: Software, Data curation. Wang Zhaofu: Writing – review & editing, Formal analysis.

Declaration of Competing Interest

We state that the manuscript titled as "The analysis and optimization of S-CO₂ coal fired power generation system using the split method" by Yuandong Guo, Enhui Sun, Jinliang Xu, Cheng Chang, Zhaofu Wang does not have any conflict of interest including any financial, personal or other relationships with other people or organizations.

Acknowledgements

This study has been supported by the National Key R&D Program of China (No. 2023YFB4102202), and the National Natural Science Foundation of China (No. 52206010, 52130608).

Data availability

Data will be made available on request.

References

- Ahn, Y., Bae, S.J., Kim, M., Cho, S.K., Baik, S., Lee, J.I., Cha, J.E., 2015. Review of supercritical CO2 power cycle technology and current status of research and development. Nucl. Eng. Technol. 47, 647–661. https://doi.org/10.1016/j. net.2015.06.009.
- Alfani, D., Astolfi, M., Binotti, M., Silva, P., Persico, G., 2024. Part-load analysis and preliminary annual simulation of a constant inventory supercritical CO2 power plant for waste heat recovery in cement industry. Energy 308, 132844. https://doi.org/ 10.1016/i.energy.2024.132844.
- Alsagri, A.S., Rahbari, H.R., Wang, L., Arabkoohsar, A., 2024. Thermo-economic optimization of an innovative integration of thermal energy storage and supercritical CO2 cycle using artificial intelligence techniques. Process Saf. Environ. Prot. 186, 1373–1386. https://doi.org/10.1016/j.psep.2024.04.094.
- Al-Sulaiman, F.A., Atif, M., 2015. Performance comparison of different supercritical carbon dioxide Brayton cycles integrated with a solar power tower. Energy 82, 61–71. https://doi.org/10.1016/j.energy.2014.12.070.
- Arslan, O., 2021. Performance analysis of a novel heat recovery system with hydrogen production designed for the improvement of boiler effectiveness. Int. J. Hydrog. Energy 46, 7558–7572. https://doi.org/10.1016/j.ijhydene.2020.11.253.
- Arslan, O., Erbas, O., 2021. Investigation on the improvement of the combustion process through hybrid dewatering and air pre-heating process: a case study for a 150 MW coal-fired boiler. J. Taiwan Inst. Chem. Eng. 121, 229–240. https://doi.org/ 10.1016/j.jtice.2021.04.012.
- Biencinto, M., Rojas, E., Bayón, R., 2021. Analysis of a hybrid dry cooling system for solar thermal electricity plants in deserts. Appl. Therm. Eng. 186, 116487. https:// doi.org/10.1016/j.applthermaleng.2020.116487.
- Chen, Z., Wang, Y., Zhang, X., Xu, J., 2020. The energy-saving mechanism of coal-fired power plant with S-CO2 cycle compared to steam-Rankine cycle. Energy 195, 116965. https://doi.org/10.1016/j.energy.2020.116965.
- Dostál, V., 2004. A supercritical carbon dioxide cycle for next generation nuclear reactors.
- Erikgenoğlu, D.K., Arslan, O., 2024. Performance assessment of Brayton-biogas multigeneration system fed by the municipal wastes. Process Saf. Environ. Prot. 188, 664–676. https://doi.org/10.1016/j.psep.2024.05.097.

- Fallah, M., Mohammadi, Z., Mahmoudi, S.M.S., 2022. Advanced exergy analysis of the combined S-CO2/ORC system. Energy 241, 122870. https://doi.org/10.1016/j. energy.2021.122870.
- Fan, Y.H., Tang, G.H., Yang, D.L., Li, X.L., Wang, S.Q., 2020. Integration of S-CO2 Brayton cycle and coal-fired boiler: thermal-hydraulic analysis and design. Energy Convers. Manag. 225, 113452. https://doi.org/10.1016/j.enconman.2020.113452.
- Feher, E.G., 1968. The supercritical thermodynamic power cycle. EnC 8, 85–90. https://doi.org/10.1016/0013-7480(68)90105-8.
- Gu, J., Liu, Q., Zhong, W., Yu, A., 2020. Study on scale-up characteristics of oxy-fuel combustion in circulating fluidized bed boiler by 3D CFD simulation. Adv. Powder Technol. 31, 2136–2151. https://doi.org/10.1016/j.apt.2020.03.007.
- Guo, J.-Q., Li, M.-J., He, Y.-L., Jiang, T., Ma, T., Xu, J.-L., Cao, F., 2022. A systematic review of supercritical carbon dioxide(S-CO2) power cycle for energy industries: technologies, key issues, and potential prospects. Energy Convers. Manag. 258, 115437. https://doi.org/10.1016/j.enconman.2022.115437.
- Hadelu, L.M., Noorpoor, A., Boyaghchi, F.A., Mirjalili, S., 2022. Exergoeconomic, carbon, and water footprint analyses and optimization of a new solar-driven multigeneration system based on supercritical CO2 cycle and solid oxide steam electrolyzer using various phase change materials. Process Saf. Environ. Prot. 159, 393–421. https://doi.org/10.1016/j.psep.2022.01.013.
- Hanak, D.P., Michalski, S., Manovic, V., 2020. Supercritical CO2 cycle for coal-fired power plant based on calcium looping combustion. Therm. Sci. Eng. Prog. 20, 100723. https://doi.org/10.1016/j.tsep.2020.100723.
- Holcomb, G.R., Carney, C., Doğan, Ö.N., 2016. Oxidation of alloys for energy applications in supercritical CO2 and H2O. Corros. Sci. 109, 22–35. https://doi.org/ 10.1016/j.corsci.2016.03.018.
- Hou, S., Wu, Y., Zhou, Y., Yu, L., 2017. Performance analysis of the combined supercritical CO2 recompression and regenerative cycle used in waste heat recovery of marine gas turbine. Energy Convers. Manag. 151, 73–85. https://doi.org/ 10.1016/j.enconman.2017.08.082.
- Le Moullec, Y., 2013. Conceptual study of a high efficiency coal-fired power plant with CO2 capture using a supercritical CO2 Brayton cycle. Energy 49, 32–46. https://doi. org/10.1016/j.energy.2012.10.022.
- Li, H., Li, Z., Lee, S., Lu, Y., Ju, Y., Zhang, C., 2024. Supercritical carbon dioxide cycle thermodynamic and exergoeconomic improvements using a bidirectional coupling strategy. Energy 296, 131140. https://doi.org/10.1016/j.energy.2024.131140.
- Liese, E., Albright, J., Zitney, S.A., 2020. Startup, shutdown, and load-following simulations of a 10 MWe supercritical CO2 recompression closed Brayton cycle. Appl. Energy 277, 115628. https://doi.org/10.1016/j.apenergy.2020.115628.
- Liu, C., Xu, J., Li, M., Wang, Z., Xu, Z., Xie, J., 2020. Scale law of sCO2 coal fired power plants regarding system performance dependent on power capacities. Energy Convers. Manag. 226, 113505. https://doi.org/10.1016/j.enconman.2020.113505.
- Liu, M., Zhang, X., Yang, K., Ma, Y., Yan, J., 2019. Optimization and comparison on supercritical CO2 power cycles integrated within coal-fired power plants considering the hot and cold end characteristics. Energy Convers. Manag. 195, 854–865. https:// doi.org/10.1016/j.enconmap.2019.05.077.
- Lu, Y., Yang, X., Bian, D., Chen, Y., Li, Y., Yuan, Z., Wang, K., 2023. A novel approach for quantifying water resource spatial equilibrium based on the regional evaluation, spatiotemporal heterogeneity and geodetector analysis integrated model. J. Clean. Prod. 424, 138791. https://doi.org/10.1016/j.jclepro.2023.138791.
- Mecheri, M., Le Moullec, Y., 2016. Supercritical CO2 Brayton cycles for coal-fired power plants. Energy 103, 758–771. https://doi.org/10.1016/j.energy.2016.02.111.
- Milani, D., Luu, M.T., McNaughton, R., Abbas, A., 2017. A comparative study of solar heliostat assisted supercritical CO2 recompression Brayton cycles: dynamic modelling and control strategies. J. Supercrit. Fluids 120, 113–124. https://doi.org/ 10.1016/i.supflu.2016.09.009.
- Narasiah, H., Kitouni, O., Scorsoglio, A., Sturdza, B.K., Hatcher, S., Katcher, K., Khalesi, J., Garcia, D., Kusner, M.J., 2024. Machine learning discovery of costefficient dry cooler designs for concentrated solar power plants. Sci. Rep. 14, 19086. https://doi.org/10.1038/s41598-024-67346-6.
- Olumayegun, O., Wang, M., Oko, E., 2019. Thermodynamic performance evaluation of supercritical CO2 closed Brayton cycles for coal-fired power generation with solventbased CO2 capture. Energy 166, 1074–1088. https://doi.org/10.1016/j. energy.2018.10.127.
- Park, S., Kim, J., Yoon, M., Rhim, D., Yeom, C., 2018. Thermodynamic and economic investigation of coal-fired power plant combined with various supercritical CO2 Brayton power cycle. Appl. Therm. Eng. 130, 611–623. https://doi.org/10.1016/j. applthermaleng.2017.10.145.
- Ramos da Costa, Y.J., Barbosa de Lima, A.G., Bezerra Filho, C.R., de Araujo Lima, L., 2012. Energetic and exergetic analyses of a dual-fuel diesel engine. Renew. Sustain. Energy Rev. 16, 4651–4660. https://doi.org/10.1016/j.rser.2012.04.013.
- Ruiz-Casanova, E., Rubio-Maya, C., Pacheco-Ibarra, J.J., Ambriz-Díaz, V.M., Romero, C. E., Wang, X., 2020. Thermodynamic analysis and optimization of supercritical carbon dioxide Brayton cycles for use with low-grade geothermal heat sources. Energy Convers. Manag. 216, 112978. https://doi.org/10.1016/j.enconman.2020.112978
- Sarkar, J., 2009. Second law analysis of supercritical CO2 recompression Brayton cycle. Energy 34, 1172–1178. https://doi.org/10.1016/j.energy.2009.04.030.
- Sun, R., Liu, M., Zhao, Y., Yan, J., 2024. Proposal design and thermodynamic analysis of a coal-fired sCO2 power system integrated with thermal energy storage. J. Energy Storage 82, 110495. https://doi.org/10.1016/j.est.2024.110495.
- Sun, E., Xu, J., Hu, H., Li, M., Miao, Z., Yang, Y., Liu, J., 2019. Overlap energy utilization reaches maximum efficiency for S-CO2 coal fired power plant: a new principle. Energy Convers. Manag. 195, 99–113. https://doi.org/10.1016/j. enconman.2019.05.009.

- Sun, E., Xu, J., Li, M., Liu, G., Zhu, B., 2018. Connected-top-bottom-cycle to cascade utilize flue gas heat for supercritical carbon dioxide coal fired power plant. Energy Convers. Manag. 172, 138–154. https://doi.org/10.1016/j.enconman.2018.07.017.
- Sun, E., Xu, J., Li, M., Li, H., Liu, C., Xie, J., 2020. Synergetics: the cooperative phenomenon in multi-compressions S-CO2 power cycles. Energy Convers. Manag.: X 7, 100042. https://doi.org/10.1016/j.ecmx.2020.100042.
- Tong, Y., Duan, L., Yang, M., Pang, L., 2022. Design optimization of a new supercritical CO2 single reheat coal-fired power generation system. Energy 239, 122174. https://doi.org/10.1016/j.energy.2021.122174.
- Turchi, C.S., Ma, Z., Neises, T.W., Wagner, M.J., 2013. Thermodynamic study of advanced supercritical carbon dioxide power cycles for concentrating solar power systems. J. Sol. Energy Eng. 135. https://doi.org/10.1115/1.4024030.
- Wang, X., Li, X., Li, Q., Liu, L., Liu, C., 2020b. Performance of a solar thermal power plant with direct air-cooled supercritical carbon dioxide Brayton cycle under off-design conditions. Appl. Energy 261, 114359. https://doi.org/10.1016/j. appergy. 2019.114359.
- Wang, Z., Sun, E., Xu, J., Liu, C., Liu, G., 2021. Effect of flue gas cooler and overlap energy utilization on supercritical carbon dioxide coal fired power plant. Energy Convers. Manag. 249, 114866. https://doi.org/10.1016/j.enconman.2021.114866
- Wang, Z., Xu, J., Wang, T., Miao, Z., Wang, Q., Liu, G., 2023. Performance of sCO2 coal-fired power plants at various power capacities. J. Clean. Prod. 416, 137949. https://doi.org/10.1016/j.jclepro.2023.137949.
- Wang, S., Zhang, Y., Li, H., Yao, M., Peng, B., Yan, J., 2020a. Thermohydrodynamic analysis of the vertical gas wall and reheat gas wall in a 300 MW supercritical CO2 boiler. Energy 211, 118611. https://doi.org/10.1016/j.energy.2020.118611.
- Wang, Z., Zheng, H., Xu, J., Li, M., Sun, E., Guo, Y., Liu, C., Liu, G., 2022. The roadmap towards the efficiency limit for supercritical carbon dioxide coal fired power plant. Energy Convers. Manag. 269, 116166. https://doi.org/10.1016/j. enconman.2022.116166.
- Wu, P., Ma, Y., Gao, C., Liu, W., Shan, J., Huang, Y., Wang, J., Zhang, D., Ran, X., 2020.

 A review of research and development of supercritical carbon dioxide Brayton cycle

- Wu, C., Wang, S.-s, Li, J., 2018. Parametric study on the effects of a recuperator on the design and off-design performances for a CO2 transcritical power cycle for low temperature geothermal plants. Appl. Therm. Eng. 137, 644–658. https://doi.org/ 10.1016/j.applthermaleng.2018.04.029.
- Xin, T., Xu, C., Yang, Y., 2020. Thermodynamic analysis of a novel supercritical carbon dioxide Brayton cycle based on the thermal cycle splitting analytical method. Energy Convers. Manag. 225, 113458. https://doi.org/10.1016/j.enconman.2020.113458.
- Xu, J., Sun, E., Li, M., Liu, H., Zhu, B., 2018. Key issues and solution strategies for supercritical carbon dioxide coal fired power plant. Energy 157, 227–246. https:// doi.org/10.1016/j.energy.2018.05.162.
- Yang, J., Yang, Z., Duan, Y., 2022. A review on integrated design and off-design operation of solar power tower system with S–CO2 Brayton cycle. Energy 246, 123348. https://doi.org/10.1016/j.energy.2022.123348.
- Zhang, Y., Li, H., Han, W., Bai, W., Yang, Y., Yao, M., Wang, Y., 2018. Improved design of supercritical CO2 Brayton cycle for coal-fired power plant. Energy 155, 1–14. https://doi.org/10.1016/j.energy.2018.05.003.
- Zhang, Y., Li, H., Li, K., Yang, Y., Zhou, Y., Zhang, X., Xu, R., Zhuge, W., Lei, X., Dan, G., 2022. Dynamic characteristics and control strategies of the supercritical CO2 Brayton cycle tailored for the new generation concentrating solar power. Appl. Energy 328, 120190. https://doi.org/10.1016/j.apenergy.2022.120190.
- Zhao, D., Deng, S., Zhao, R., Zhao, L., Xu, W., Long, X., 2021. The flexible programming of thermodynamic cycles: application of supercritical carbon dioxide Brayton cycles. Energy Convers. Manag. 245, 114624. https://doi.org/10.1016/j. enconman.2021.114624.
- Zhou, J., Zhang, C., Su, S., Wang, Y., Hu, S., Liu, L., Ling, P., Zhong, W., Xiang, J., 2018. Exergy analysis of a 1000 MW single reheat supercritical CO2 Brayton cycle coal-fired power plant. Energy Convers. Manag. 173, 348–358. https://doi.org/10.1016/j.enconman.2018.07.096.